JOURNAL OF PROPULSION AND POWER
Vol. 27, No. 1, January–February 2011

Emissions and Thermodynamic Performance Simulation of an Industrial Gas Turbine

Elder Marino Mendoza Orbegoso,* Cláudia Domingues Romeiro,† Sandro Barros Ferreira,‡ and Luís Fernando Figueira da Silva§
Pontifícia Universidade Católica do Rio de Janeiro, 22453-900 Rio de Janeiro, Brazil

DOI: 10.2514/1.47656

This paper presents the results of a study on the influence of the fuel gas composition on the thermodynamic performance of a typical heavy duty gas turbine, followed by an emissions prediction using a chemical reactor network which, in its turn, uses one of the most developed chemical kinetic mechanisms for the natural gas combustion. The first part of this work regards a statistical analysis of a time series, which shows the fuel gas composition variation along a certain period, revealing the typical concentrations of the gas species. Based on the curves provided by the statistics, several gas compositions were proposed and applied to a thermodynamic model to evaluate the impact of the species composition of the natural gas on the gas turbine heat rate and power. Afterward, several approaches of chemical reactor network were considered to choose the methodology that better predicts the temperature and CO and NOx formation within a gas turbine combustor operated at base load regime. Finally, the influence of the natural gas composition variation over the aforementioned thermochemical properties at the exit of the combustion chamber when considering both operation regime and combustor's natural gas composition was studied.

I. Introduction

THE modeling of the combustion systems in energy conversion equipments, such as gas turbine combustors, has many challenges especially concerning the limitations of the predictive capacity of the models based on the computational fluid dynamics (CFD) and their associated computational cost. Thus, when compared with these more elaborate techniques, models based on chemical reactor network (CRN) ally the low computational cost with the ability to predict pollutant emissions, however, without the descriptiveness of the dynamics of the reacting flow. So, because the advent of the jet engine, the modeling based on the CRN approach has been an essential tool in the analysis, design and optimization of practical combustion systems, particularly with the purpose to ensure an efficient operation coupled with low emissions of pollutants.

The CRN approach consists in the resolution of simplified transport equations to describe the operation of trivial combustion models such as perfectly stirred reactor (PSR) and plug flow reactors (PFR), which are systematically arranged into a structured scheme with the purpose to represent the combustion process occurring within combustion equipment. This approach is very useful in the prediction of relevant thermochemical properties such as temperature and pollutants emissions, which are the most significant parameters in the operation of those equipments. This is the reason why the choice of a detailed kinetic mechanism, that represents the oxidation of any fuel involved in the combustion of gas turbines, requires a prior identification of the associated validity range.

An experimental study was developed [1] concerning the determination of NOx formation as a function of the fuel hydrocarbon in premixed-lean combustion. In this study, an atmospheric pressure jet stirred reactor (JSR) operating at 1788 K was used to determine the influence of hydrocarbon type over the NOx concentration ranging from methane (C1) to *n*-hexadecane (C16). An increase in NOx production was observed as the alkanes fuel ranged from C1 to C5. Subsequently an independence of the NOx formation as the fuel molecule goes from C5 to C16 was shown to exist.

A similar study [2] measured NOx as a function of C/H ratio given by the use of methane, ethylene and several mixtures of C1–C4 hydrocarbons in the operation of a lean-premixed JSR at atmospheric conditions and temperature of 1790 K. The results supported those of [1], i.e., the increase in NOx content as the C/H ratio is increased. Furthermore, the results were used as a basis of comparison for the numerical modeling of the JSR, by the use of two different CRN models, both numerical results were in agreement with those obtained experimentally.

Experimental results [3] were also obtained of the influence of natural gas composition on the NOx formation in a microturbine generator. For this study, the turbine exhaust temperature was maintained constant at 635°C where the temperature of preheated air and the pressure ratio at the exit of the compressor were fixed to 565°C and 4:1, respectively. It was shown that under the fixed load conditions, where the N_2O and prompt NOx mechanisms prevail over the thermal NOx mechanism, NO concentration decreases when methane concentration in the natural gas increases.

The principal aim of this work is to determine, for different operating conditions, the influence of natural gas composition on energetic and emissions performance of an industrial gas turbine at fixed compressor outlet conditions. For this purpose, this paper is composed of four sections. In the second section, a linear regression statistical analysis is applied to a data set corresponding to the natural gas composition that is daily provided to an industrial gas turbine installation, to establish the variations of each hydrocarbon and the plausible range to be analyzed. Afterward, a model was built in thermodynamic software is used to estimate the temperature and the pressure values after the combustor, as well as providing the input parameters to the model based on chemical reactor network approach in the description of combustion process for an industrial Dry Low NOx (DLN) turbine combustor.

In Sec. III, a literature review is presented for several existing natural gas detailed kinetic mechanism, to provide for an insight of those schemes that are the most reliable in describing the combustion

Presented as Paper 2009-5210 at the 45th AIAA/ASME/SAE/ASEE Joint Propulsion Conference & Exhibit, Denver, CO, 2–5 August 2009; received 15 November 2009; revision received 1 September 2010; accepted for publication 21 September 2010.

*Graduate Student, Department of Mechanical Engineering, Rua Marquês de São Vicente, 225.
†Research Engineer, Institute of Energy, Rua Marquês de São Vicente, 225.
‡Research Engineer, Institute of Energy, Rua Marquês de São Vicente, 225.
§Visiting Professor, Department of Mechanical Engineering, Rua Marquês de São Vicente, 225. Senior Member AIAA.

process over the operation parameters within of range of interest. After having chosen the most appropriate natural gas mechanism, three CRN configurations are built to determine the one that best describes the combustion process of that typical DLN combustor, particularly envisaging the most appropriated NOx pollutant estimation description.

The fourth section describes the results obtained with the CRN approach, under three operation conditions (one at base load and two at part load regime) to determine the influence of the natural gas composition on the temperature, as well as on CO and NO emissions at the exit of such a combustor. Also, it is determined the influence of the feeding system on these thermochemical parameters.

Finally, conclusions are formulated based on the results obtained.

II. Analysis of Natural Gas Composition

The natural gas is one of the simplest and most used fuels in the planet, being composed largely of methane, although minor quantities of heavier hydrocarbons such as ethane, propane, butane, pentane, hexane, and other inert species as carbon dioxide and nitrogen are present.

The natural gas composition that is provided to an existing power plant exhibits variations in time, what motivates an investigation of the influence of these alterations on the pollutant emissions. A statistical analysis of the natural gas composition was performed for a 489 days period, at the site of a combined cycle power plant.

Figure 1 shows the measured conditional probability density functions (PDFs) of the concentration of all the hydrocarbon species as a function of methane volume fraction. It allows to verify the nontrivial nature of these PDFs, which present a bimodal nature. In particular, the methane PDF exhibits a bias toward large concentration values and a large tail toward the smaller ones. Note that typical excursions in methane molar fraction lie in the 92–98% range, this variability will be considered on the combustion calculations in the following sections.

Figure 2 shows the scatter plot of the composition of the all species contained in the natural gas against the methane. This figure demonstrates a decreasing linear tendency of all the minority species when the methane increases. A linear correlation higher than 0.80 of all the minority species against the methane by least squares fit, also shown in this figure, is representative of the variability of all the species contained in the natural gas with the exception of the hexane.

Even if alternative analysis could be envisaged, such as the response surface map, the simple linear regression is deemed sufficient for the present purposes. Table 1 shows the resulting least squares coefficients.

III. Thermodynamic Performance

The second part of this work regards the simulation of the thermodynamic performance of the gas turbine engine as the fuel gas composition is changed. The simulation departs from the gas turbine

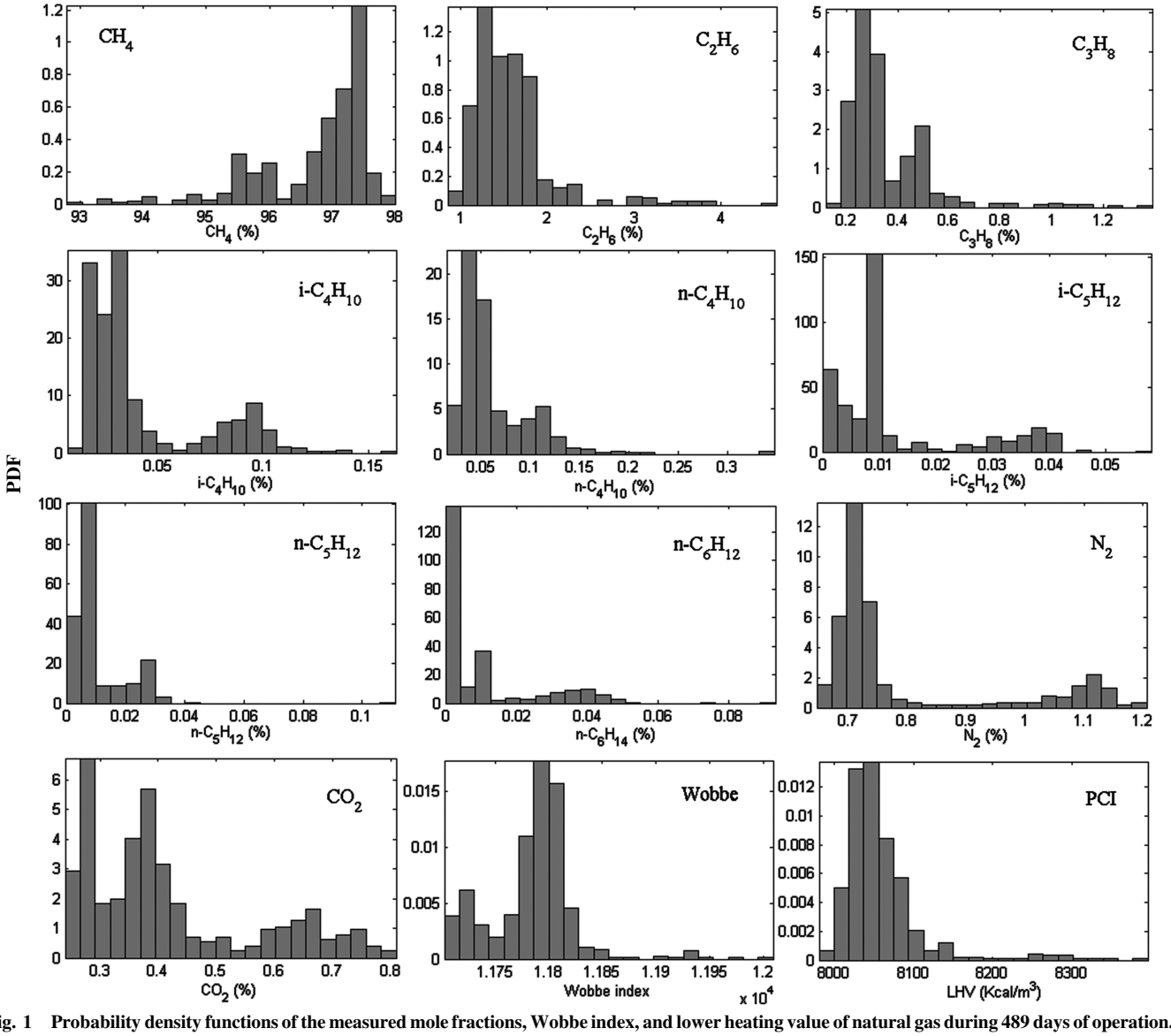

Fig. 1 Probability density functions of the measured mole fractions, Wobbe index, and lower heating value of natural gas during 489 days of operation.

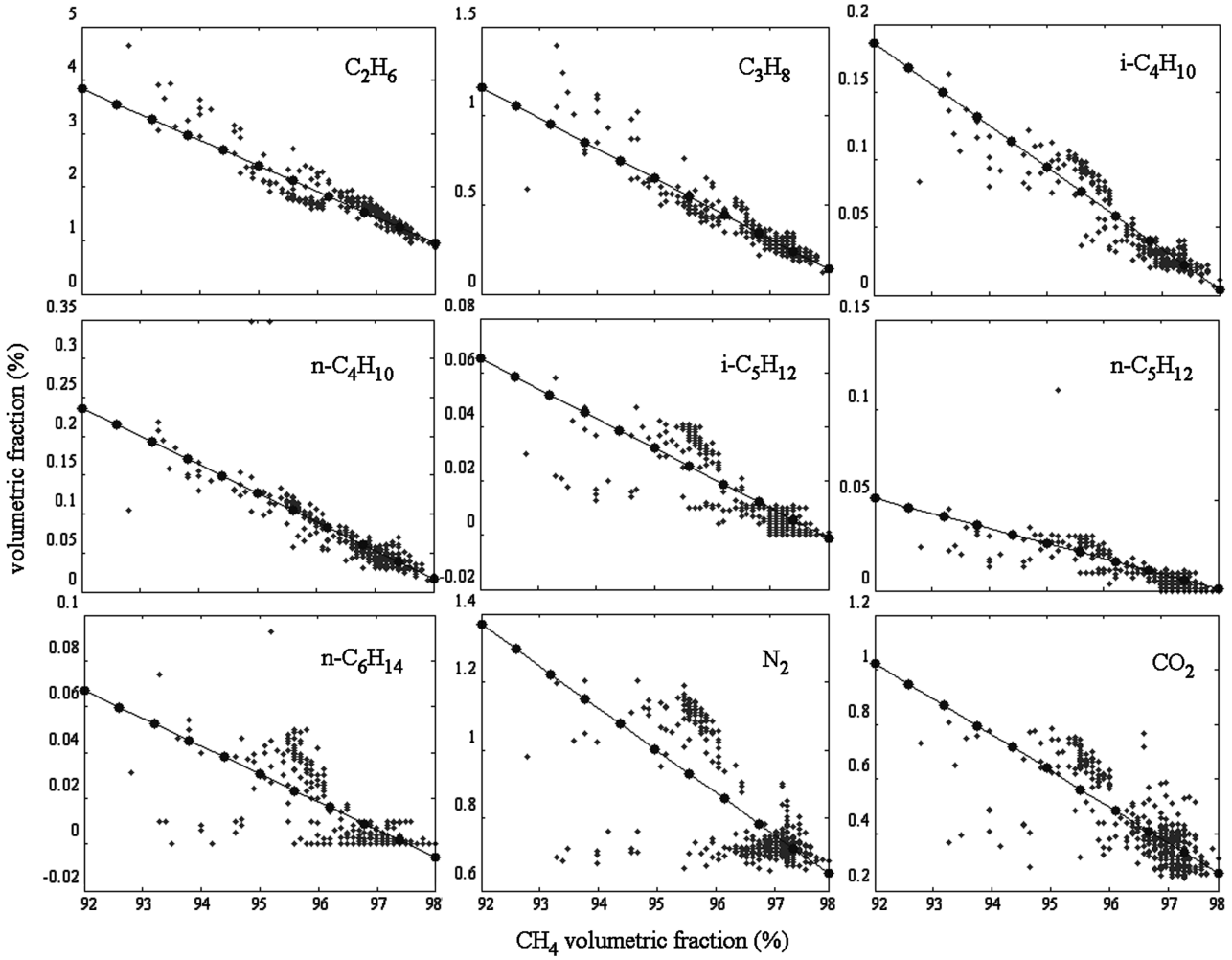

Fig. 2 Concentration of different species present in the natural gas as a function of methane concentration. The lines are least squares fits.

engine design data, shown in Table 2, to adjust the main parameters of the engine within the model. The software used in the simulations is GateCycle [4], a proven simulation tool.

Having adjusted the numerical model for the design point, a simulation of the engine at three representative operating points was conducted which results are shown in Table 3. The variation of the fuel gas composition has been accounted for through the lower heating value. Compressor performance is calculated based on a map of characteristics available in GateCycle™.

IV. Assessment of Combustion Chemistry Mechanisms for the Natural Gas

Even for the simplest hydrocarbons, like methane, that has been studied for more than four decades, does not exist any complete neither unified kinetic scheme that can simulate their oxidation in a broad range of parameters (i.e., pressure, temperature and equivalence ratio). When heavier hydrocarbons (such butanes, heptanes, etc.) and/or mixing of hydrocarbons (like natural gas, liquefied petroleum gas, etc.) are considered, the validation range decreases considerably. This problem occurs mainly due to the large number of degrees of freedom and the possible pathways of reaction in the description of the oxidation of fuels, particularly for lower temperature range, for which the chemical kinetic mechanisms is less studied. Thus, the usage of existing combustion mechanisms demands, a priori, the knowledge of their associated validation range [5]. For the specific case of the natural gas, a set of elementary

Table 1 A, B constants and correlation coefficients by $[E] = A * [CH4] + B$ equation, obtained from least square fits

Linear regression constants			
Species (E)	A	B	Correlation coefficient
C_2H_6	−0.4795	47.9535	−0.9116
C_3H_8	0.1699	16.7901	−0.913
i-C_4H_{10}	−0.0304	2.9849	−0.9174
n-C_4H_6	−0.0366	3.6063	−0.8592
i-C_5H_{12}	−0.011	1.0813	−0.7994
n-C_5H_{12}	−0.0084	0.8202	−0.7542
n-C_6H_{14}	−0.0121	1.1812	−0.7129
N_2	−0.122	12.5937	−0.6871
CO_2	−0.1284	12.8342	−0.7668

Table 2 Design point parameters for the simulated gas turbine engine

Design parameters	
Ambient temperature, K	288.15
Ambient pressure, bar	1.01325
Relative humidity, %	60
Compressor inlet pressure drop, kPa	0.846
Exhaust pressure drop, kPa	1.244
Exhaust temperature, K	867.18
Exhaust flow, kg/s	457.45
Fuel flow, kg/s	9.94
Compressor isentropic efficiency	0.86
Combustion efficiency	0.96
Turbine isentropic efficiency	0.92
Net power, MW	183.37
Thermal efficiency	37.48
Overall pressure ratio	16.4

Table 3 Input parameters for chemical kinetics simulation

Input parameters	Unit	Base load	Part load II	Part load II
Ambient temperature	K	293.06	300.32	298.67
Ambient pressure	bar	1.01	1.00	1.01
Relative humidity	%	86.67	78.83	87.50
Fuel flow	kg/s	9.68	8.55	8.68
Low heating value	kJ/kg	48.246	48.759	48.246
Exhaust temperature	°C	592.02	598.34	585.91
Power output	MW	169.17	144.01	149.15

reaction and chemical species that comprehends a detailed kinetic mechanism for this specific fuel must cover the hydrogen oxidation mechanism as well as the chemical kinetic of C1-C3 hydrocarbons, which frequently, are arranged in a hierarchical structure, having as a basis the H_2 and CO oxidation mechanisms.

Several detailed kinetic mechanisms for the description of natural gas combustion are reviewed here, emphasizing the advantages and the drawbacks of every mechanism as well as the range operation that are able to predict, with a certain degree of confidence, the thermochemical parameters of interest such as ignition/extinction, residence time, flame laminar velocity, autoignition delay time, temperature and species profiles, etc., when is applied to simplified physics systems.

The development of the detailed chemical kinetic mechanism for the natural gas combustion began in the 1970s, when several high-temperature kinetic models for the hydrogen, carbon monoxide and methane oxidation were constructed under the support of large quantity of experimental data [6,7]. During the early 1980s, it was proposed the first chemical mechanism for combustion of the C1 and C2 hydrocarbons that was composed of 93 reversible elementary reactions and 26 chemical species [8]. This mechanism was subsequently revised in [9] by adding elementary reactions to the C1 and C2 submechanisms. The authors also suggested the inclusion of C3 elementary reactions to get an accurate numerical description of methane combustion. Later, in [10], it was developed and enhanced the mechanism of [8] for the ethylene combustion, where the elementary reactions were increased to 162, increasing simultaneously the validation range for the combustion simulation in shock tubes for the methane, ethane and ethylene.

The compilations of [11,12] were the starting point in the development of the nitrogen oxidation mechanisms. Later, two compilations were published [13,14] concerning the updated rate coefficients for many elementary reactions relevant to the oxidation of simple fuels. Recently, these compilations were newly updated and expanded [15] on the basis of recent theoretical and experimental studies of elementary reactions.

In [16], a set of systematic procedures was proposed which should be observed to develop a comprehensive chemical kinetic mechanism for any fuel. These recommendations were followed for the construction of the most recognized kinetic models such as the GRI[¶] and Leeds [17] mechanisms.

The GRI mechanism, developed to describe the methane oxidation [18][**] is based on a set of elementary reactions, where the attributed values for the reaction rate parameters are provided through the association of theoretical, experimental, and numerical data. Early versions of the GRI-Mech were constituted by 32 species and 177 reverse chemical reactions and originally built for the description of the methane combustion without considering the nitrogen oxidation. This mechanism was subsequently updated to the GRI-Mech 2.11[††], that takes into account the kinetics of the nitrogen oxidation, so the species number was increased to 49, involving 279 chemical elementary reactions.

The GRI-Mech 3.0 is the latest version currently available which was built for the combustion of the natural gas as a mixture of ethane, methane and propane. This version considers 53 species and 325 elementary reactions. This mechanism is able to correctly predict the oxidation of the natural gas as well as their hydrocarbon components (up to propane) when several combustion systems, i.e., PFR, shock tube, stabilized burning flame, etc., are considered. The validation range covers the 1000–2500 K of temperature, 0.015–10 atm of pressure and 0.1 to 2.5 of equivalence ratio.

The most relevant advantage of GRI-Mech is the good representation of the majority of experimental results available for the natural gas combustion, as well as their most relevant constituents, as methane and ethane, although this is only verified when application conditions are close to laboratory conditions. The absence of hierarchy is the principal drawback of the GRI-Mech that leads to the inability in shifting new kinetic parameters without retuning when accurate experimental data become available [17], and the awkwardness in developing new mechanisms for other heavier hydrocarbons taking the GRI-Mech as a building block.

The Leeds [17] mechanism models the oxidation of the higher gaseous fuels such as methane, ethane, ethylene, acetylene, carbon monoxide and hydrogen, in a broad range of operational parameters. This mechanism was built in a similar manner to the GRI-Mech, namely, by means of the usage of gas kinetics measurements. These mechanisms have, as their construction base, a similar set of experiments concerning the laminar burning velocity, ignition delay time and the species profiles in premixed laminar flames. The Leeds mechanism also was developed using kinetic data published in [13,14].

The Leeds Methane mechanism 1.5 [19] consists of 351 irreversible elementary reactions and 37 chemical species, and does not consider the nitrogen oxidation mechanism. The Leeds Methane, NOx and SOx mechanism [17], takes into account both the nitrogen and sulfur oxidation kinetics which includes 78 species and 892 irreversible (450 reversible) reactions. This mechanism accurately predicts the laminar burning velocity of methane/argon and ethane/argon mixtures at standard conditions of pressure and temperature (1 atm and 298 K, respectively) and when the equivalence ratio ranges within 0.6 and 1.4. This mechanism is also able to simulate the ignition delay time of methane/oxygen and ethane/oxygen mixtures diluted in argon in the range of 1–29 atm of pressure, 1500–2050 K of temperatures and 0.5–2 of equivalence ratio [19]. The Leeds mechanism is less restrictive than the GRI-Mech when a comprehensive mechanism for heavier hydrocarbons is intended to be built, i.e., it is possible to develop a kinetic model for heavier hydrocarbons from the Leeds methane mechanism without the alteration of the elementary kinetic reaction data [20].

The Konnov kinetic mechanism also simulates the natural gas combustion, as well as the C2–C3 hydrocarbons combustion, the hydrogen oxidation, and the NOx formation in flames. This mechanism was developed on the basis of the methane mechanism developed in [21], where important extensions were taken into consideration as the methanol and ethanol mechanisms [22,23] the NOx mechanism from [11] and the CEC compilations kinetic data [13,14].

The Konnov 0.5 mechanism [24] accounts for 127 chemical species and 1200 elementary reactions. It was extensively validated by comparisons against experiments of delay ignition time, species profiles on premixed laminar flames, laminar burning flame velocity and the temperature and species profiles on plug flow reactor system. Nonetheless, the majority of the validations documented were focused on the kinetics of H_2, CO, N_2O, NO_2, NH_3 and Syngas. To the best of our knowledge the work of [25] is the only reference found in the validation of the Konnov's mechanism [24] for the methane combustion, when ignition delay time is considered.

The San Diego mechanism (CERMECH) is based on the principle in which a kinetic mechanism must include only a moderate number of species and reactions that are representative in the description of several fuels as methane, methanol, ethane, ethylene, ethanol, propane, and propylene. A version 20050310 of the San Diego mechanism [26], includes 37 species and 177 elementary reactions. This version was built upon the basis of previously tested and

[¶]Data available online at http://www.me.berkeley.edu/gri_mech/ [accessed May 2008].

[**]Data available online at http://www.me.berkeley.edu/gri_mech/ [accessed May 2008].

[††]Data available online at http://www.me.berkeley.edu/gri_mech/ [accessed May 2008].

validated submechanisms such as the hydrogen and CO oxidation [27–29] followed by the addition of schemes developed by several authors for the representation of the combustion of the methane, methanol, ethane, ethylene, and acetylene. In addition to the proficiency of the San Diego 20050310 concerning the prediction of the combustion of C1–C2 hydrocarbons, this version is capable in estimating the ignition delay time for C3 hydrocarbons within the range of 1000–2200 K of temperature, 1–30 atm of pressure and 0.5–2 of equivalence ratio. The laminar flame velocity of C3 hydrocarbon at standard conditions is another parameter that this mechanism can estimate in an efficient way.

A kinetic mechanism for the combustion of C1–C6 hydrocarbons was developed in [30–35]. The last version [35] is formed by 883 reversible elementary reactions involving 121 chemical species. This mechanism, in opposite to the GRI-Mech, [18] has a hierarchically structure, namely, it was sequentially developed starting from the hydrogen oxidation mechanism up to the heaviest hydrocarbons submechanisms.

The mechanism was shown to be able to predict 1) the premixed laminar burning velocity for C1–C3 alkanes at ambient conditions, 2) the ignition delay time of natural gas at stoichiometric conditions and at low pressures, and 3) the oxidation of the 10:1 mixture of methane and ethane in a PSR at 1–10 atm of pressure and over a broad range of equivalence ratio [34]. However, this is a restricted availability mechanism.

Le Cong and Dagaut [36] developed a kinetic mechanism, initially formed by 737 reversible reactions and 98 chemical species, herein called L&D mechanism, which allows to simulate the natural gas and Syngas combustion within a 1–10 atm, 911–1400 K and over an extensive range of equivalence ratios. This mechanism was built upon the mechanism developed in [37] for the combustion of the natural gas. The systems used in the validation of this mechanism include shock tubes, premixed laminar flames, PSRs and PFRs, where excellent agreements were found with experimental data registered in the literature.

Le Cong and Dagaut [38] extended their previous mechanism to estimate the combustion of mixtures of hydrogen and natural gas diluted with water vapor. This last version, the L&D 2.0 mechanism, contains 128 chemical species and 924 elementary reversible reactions. The validation was performed for methane combustion diluted in 1–10% on water vapor within a PSR at residence time of 120 ms, whose operation parameters corresponds the 1000–1300 K, 0.2–2 of equivalence ratio and at atmospheric pressure.

This mechanism is also able to describe the hydrogen and the monoxide carbon oxidation, as well as the lighter hydrocarbons, such as methane, ethane, methanol, formaldehyde and mixtures of those, like natural gas in pure state or diluted in vapor water. These fuels were simulated in several combustion situations, such as PSRs, PFRs, shock waves, premixed laminar flames, etc., so that this kinetic mechanism was extensively validated and compiled in the work of [39].

Petersen et al. [40] developed a detailed kinetic mechanism with the main purpose of describing the natural gas oxidation at high pressures as a combination of C1–C3 mixtures. More recently, this mechanism was extended [41] to the combustion of C1–C5 type hydrocarbons, and now it consists of 1380 reactions and 230 species. Configurations of shock tube and rapid compression machine operating at pressures up to 50 atm, and over the broad range of temperature and equivalence ratio, were used as experimental tools for the validation of this mechanism. Simulation results were compared experimental autoignition delay times for the combustion with air of hydrocarbons compositions representative of natural gas, methane/propane [42], methane/ethane/propane [43], methane/*n*-butane [41], and methane/ethane/propane/*n*-butane/*n*-pentane [44]. The results of these comparisons demonstrated the good reliability of this mechanism on the prediction of the gas natural autoignition delay time at elevated pressures. Therefore, their use in the prediction of the autoignition delay time in the oxidation of several C1–C5 hydrocarbons is undoubtedly guaranteed.

Almost all the aforementioned detailed chemical kinetic mechanisms have been compared with recent experimental data obtained for laminar flames and stirred reactors [45]. Those comparisons show that L&D mechanism is the one which better predicts stirred reactor results, even if it maybe argued that the value of the heat of formation of OH is incorrect [46] or that a simplified treatment of $H + O_2 + M \Leftrightarrow HO_2 + M$ reaction is used when compared with other mechanisms as the Galway NC5-49 [44]. Because such reactors are representative of the PSR which are used to model combustion here, the 10 atm L&D mechanism will be adopted in that follows. Note that the application of a mechanism which was validated for a pressure of 10 atm to predict combustion at 15 atm is subject of caution.

V. Reactor Network Modeling Techniques

A complete description of the combustion processes needs a simultaneous solution of the laws that govern the fluid mechanics and reaction kinetics, and its complexity increases as grows the number of species and reactions of a kinetic mechanism in question. Thus, the direct incorporation of a detailed chemical kinetic of combustion to a CFD code is still impracticable, in terms of the computational burden [47], because the solution of hundreds of coupled differential equations within thousands of elementary control volumes would be required.

A first approach that aims the attenuation of the computational effort in the simulation of practical combustion systems, such as a gas turbine combustor, consists in the simplification of the chemical kinetics description while retaining the fluids mechanics description. This simplification involves a set of reduced elementary reactions and chemical species; however, the reduced schemes are valid only within a narrow range of pressure, temperature and composition, in which the reduced mechanism is capable to simulate, not being able to represent in detail the chemical process [5].

The CRN is an alternative to the simulation of gas turbine combustors, because it simplifies the fluid mechanics descriptions while keeping the details of the chemical kinetic description. This approach considers the resolution of idealized physical systems as representative of the operation of devices frequently used in continuous chemical processes such the PFR and the PSR. While the PFR model assumes that the confined fluid moves through plugs, as a result of the absence of axial diffusion, the PSR model considers the mixing among reactants and products as being homogeneous and instantaneous.

The principal advantage in the simulation of gas turbine combustors by mean of the CRN approach is the relatively low computational cost, when compared with the CFD approach. However, this benefit appears as a detriment to a detailed description of the flow within the domain under analysis. To develop a model that simulates the operation of a gas turbine combustor which considers the CRN approach, several hypotheses must be made, which aim to reduce the complexity of the governing equations related to the fluid mechanics, while retaining the information concerning to the kinetics of the combustion.

Thus, with the usage of the CRN approach, it is possible to obtain an accurate description of the combustion process in confined regions of a gas turbine combustor. For this purpose, it is required the use of PSR and PFR models, which must be linked in a systematic and structured arrangement. The PSR models are used in the description of the combustion processes occurring in the flame/ignition (or primary) zone of the combustor, whereas PFR models simulate the combustion in the intermediate and dilution zones.

In this work, three different configurations will be considered, which differ from each other by the arrangement of PSRs used in the representation the primary zone of the combustor. These arrangements will be developed to underscore those that would be capable of yielding accurate emission predictions in the operation of the gas turbine at base load and part load conditions.

Figure 3 shows the basket of the combustion chamber, which was designed with the purpose of establishing appropriate conditions to maintain the combustion processes in an efficient and stable way, and thus the chemical and mixing turbulent are most relevant before the convective process. The link between the basket and the turbine is

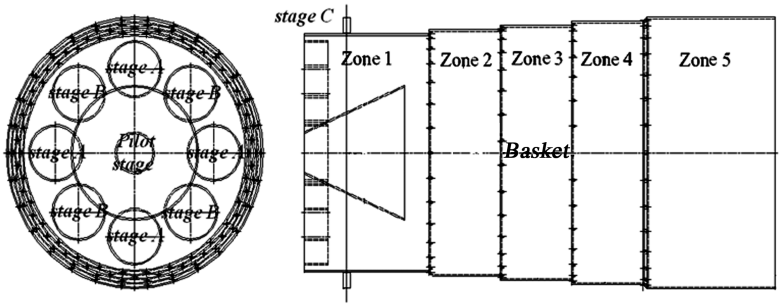

Fig. 3 Simplified geometric representation of the combustor modeled.

made through a straight transition piece, not shown here, which redirects the exhaust gases from the basket to dilute with fresh air up until allowed temperatures are reduced at the first stage expansion of the turbine. Table 4 summarizes the measured volume occupied by the fluid at each of these zones.

At base load operation, a high percentage of the fuel supplied to the combustor is premixed with air at lean conditions, the chemical reaction occurs in a narrow region of equivalence ratio and closer to the lean flammability limit. Consequently, the combustion temperature in the primary region and the NOx emissions at the combustor exit is expected to be reduced. To make this possible, the combustor uses four feeding systems called stages (A, B, C, and *pilot*). Stage C corresponds to an ultra lean premixed fuel and air upstream to the combustion chamber.

Stages A and B admit natural gas to the primary zone by eight premixing nozzles, four for each stage, where the natural gas continuously mixes with a ultra lean premixed air and natural gas, that is previously injected in the stage C. The primary function of the *pilot* stage is to produce a turbulent flame with the purpose of assuring a high combustion temperature (2000–2200 K) and maintaining a stable flame.

Figure 4 shows a schematic representation of the first configuration, which corresponds to the modeling of a typical gas turbine combustor. In this configuration, the single PSR that models the combustion in the primary zone is continuously fed by the premixed air and natural gas as reactants. It is assumed that, the zones 2, 3 and 4, shown in Fig. 3, corresponds to the combustion primary zone. The intermediate zone matches the geometric zone 5 of the basket and the dilution zones are considered to be occupied by the whole inner volume of the transition piece.

After the burning gases leave the PSR, they are diluted with air before entering the intermediate zone that is simulated by a PFR model. Finally, the products that leave the first PFR are again diluted with air before they step into the dilution-cooling zone that is also described by a second PFR model. The adoption of PFRs in the modeling of the combustion in the intermediate and dilution-cooling zones of a combustor is due to the presumed negligible influence of the transport by diffusion of all chemical species relative to the combustion of the burned gases from the primary zone, when compared with the longitudinal transport. Such an arrangement of reactors described for the first configuration (shown in Fig. 4) is frequently used in simulations of combustors [48–52].

Nevertheless, the adoption of a single PSR as being a representative model of the combustion process in the flame/ignition zone of gas turbine combustors is not always appropriate due to the complexities associated to the flowfield, as well as the details on the feeding of oxidizer and fuel in that zone. Therefore, in [53] it was developed an alternative approach for the modeling of the flame/ignition zone of a gas turbine combustor to predict the CO and NOx emissions in the operation of aeroderivative gas turbines.

Table 4 Volumetric characteristics for the gas turbine combustion chamber

Entrance Parameters		Units	Value
Volume (zones)	1	dm^3	10
	2	dm^3	6
	3	dm^3	6.4
	4	dm^3	6.8
	5	dm^3	13.3
	Transition piece	dm^3	46

This approach consists in the division of the primary zone in equally spaced regions, as can be seen in Fig. 5. The combustion process at each region is represented by a single PSR operating with the similar pressure and temperature inlets; however, the equivalence ratio is assigned to each reactor in accordance to a Gaussian distribution by the unmixedness parameter S [54] defined as the ratio between the representative equivalence ratio in the primary zone of the combustor μ_φ and the corresponding standard deviation σ_φ. In this manner the unmixedness process is taken into account, which is the main responsible of the NOx formation in gas turbine combustors [54].

In accordance to the experimental data collected in [54], the maximum value of S in the primary zone that is expected to occur is equal to 0.7. Note that, when $\sigma_\varphi = 0$ this approach corresponds to the modeling to the primary zone by the adoption of a single PSR, thus recovering the situation described in Fig. 4, where the unmixedness was neglected.

This methodology also establishes the number of PSRs that should be considered for the equivalence ratio distribution, which should be determined as function of the percentage change of NOx and CO emissions index as result of progressive increments of PSRs arranged in parallel [53]

$$\%\Delta[\mathrm{CO}]_{(i+1)} = 100 \times ([\mathrm{CO}]_{(i+1)} - [\mathrm{CO}]_{(i)})/[\mathrm{CO}]_{(i)} \quad (1)$$

$$\%\Delta[\mathrm{NOx}]_{(i+1)} = 100 \times ([\mathrm{NOx}]_{(i+1)} - [\mathrm{NOx}]_{(i)})/[\mathrm{NOx}]_{(i)} \quad (2)$$

where i refers the number of PSRs in the primary zone and the values of [CO] and [NOx] concentrations is obtained by the previous simulation of the gas turbine combustor considering i and $i + 1$ PSRs in the primary zone, respectively. The numerical results of this set of equations limit the number of PSR that should represent the combustion in the primary zone, specifically, when the variation of the calculated CO and NOx emission must be within the uncertainties in the experimental emissions data. In [54] it is recommended the conservative values of 5 and 15% for $\%\Delta$[NOx] and $\%\Delta$[CO], respectively, when the CRN modeling for aeroderivatives gas turbines combustor is considered.

Because of the calculated CO and NOx emissions are strongly dependent on the unmixedness, the adequate determination of this parameter is vital in the correct prediction of the emissions. A recommended manner in the determination of S is by the assumption that this parameter is only function of the primary zone mean equivalence ratio and is independent of the combustor geometry. Allaire et al. [53] fitted a general curve from experimental data collected by [55] taking into account several geometric configurations of combustion chambers, which allows to estimate the unmixedness as function of the primary zone mean equivalence ratio.

Finally, the postcombustion zones were modeled in the same way that those described in the first configuration, i.e., by the adoption of

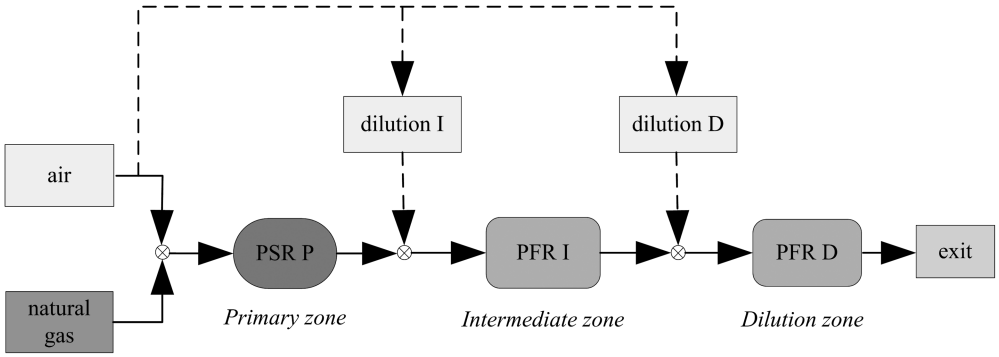

Fig. 4 Schematic representation of the classical reactor network approach.

PFR reactors as the best way of representing the thermochemical process in the intermediate and dilution-cooling zones.

A third configuration in the modeling of an industrial gas turbine combustor by the CRN approach is considered in this work as an alternative to the two previously described to represent the combustion process in the primary zone and, consequently, a better estimate of the thermochemical properties at the exit of the combustion chamber.

As can be seen in Fig. 6, the primary zone combustion is modeled taking into consideration the operation parameters that are typical for each inlet systems (stages). The intermediate and dilution zones were modeled as the same way as the two aforementioned configurations.

VI. Results and Discussion

A. Assessment of the CRN Configurations in the Emissions Predictions

This section presents the simulation results of the three aforementioned reactor network configurations, operating at base load conditions. This preliminary simulation was performed as a way of assessing the CRN approach that more accurately represents the thermochemical process at the exit of the combustion chamber, i.e., at the exit of the transition piece, to use it for several gas turbine operation regimes.

The software used for this simulation was the Chemkin™ 4.1 whereas the L&D 2.0 [38] natural gas mechanism was adopted for the CRN simulation. The choice of L&D 2.0 mechanism was performed on a basis of the most recent bibliographical study for the NG mechanism previously addressed in this work, where the results of that study reveals the L&D 2.0 is the kinetic scheme that better reproduces the process of combustion of PSR models operating at conditions representative of gas turbines [40].

Table 5 shows the global operation parameters of the gas turbine operating at base load regime (169.17 MW) to be considered in the simulation of the combustion process using the three aforementioned CRN configurations. It is worth to emphasize that the models of the intermediate and the dilution zone are similar for these three configurations, differing only in number and arrangement of PSRs that was adopted for the modeling of the primary zone.

The results of these simulations were compared with those obtained from the thermodynamic cycle analysis using the GateCycle™ software and the field data, leading to a choice of reactor volumes (or, equivalently, of residence times) in each combustion zone previously determined which best reproduces the computed temperature and the measured CO and NO volume fractions at the exit of the combustion chamber, i.e., immediately upstream to the beginning of the first stage expansion process. Once computed, these volumes, which are given in Table 6, are kept

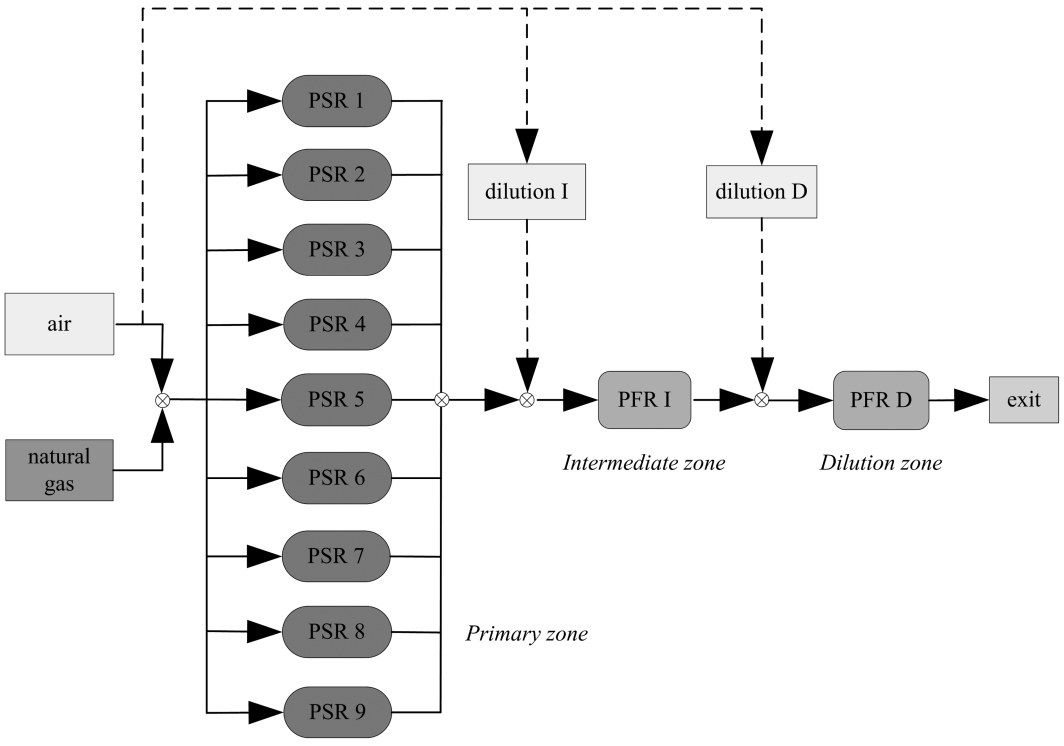

Fig. 5 Schematic representation of the reactor network analogous to that proposed in [46] in the primary zone modeling for the gas turbine combustor.

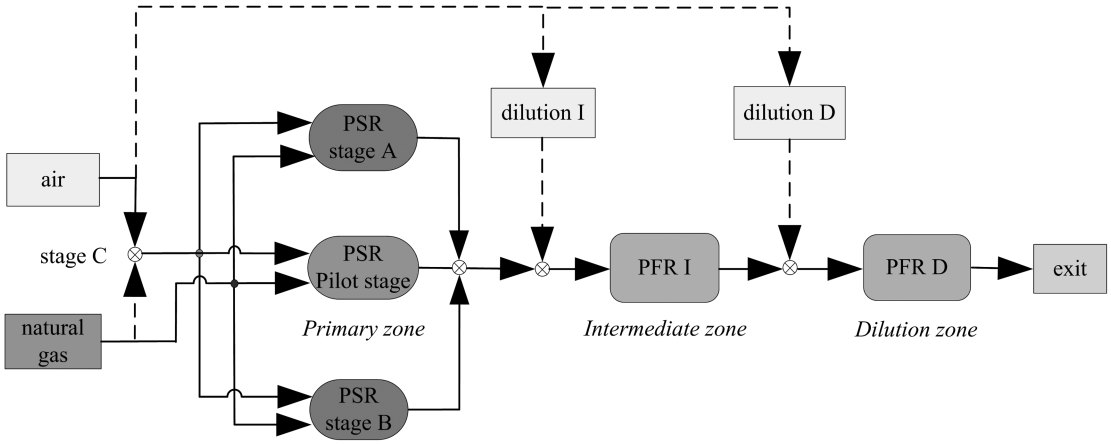

Fig. 6 Schematic representation of the reactor network approaches proposed in this work for the primary zone modeling for the gas turbine combustor.

constant throughout the computations. Since these volumes are modeled by PSR, previous PSR comparisons [40] indicate that an analysis of the mechanism on the computed results is not necessary here.

Table 7 displays the results at base load condition of the gas turbine (169.17 MW), of the thermochemical parameters obtained by the simulation in Chemkin™ using the three CRN configurations, in comparison with: 1) the burnt gases temperature at the end of the combustion process estimated by the use of GateCycle™software, and, 2) the CO and NO concentrations acquired by the monitoring measurements of that gas turbine.

As can be seen in Table 7, the temperature of burnt gases at the end of the combustion chamber is better estimated by the use of the first and the third CRN configurations, whereas the second methodology overpredicts by about 20 K the temperature at the end of the combustion process obtained by the thermodynamic cycle simulation. In the same manner, the predictions of the NO concentration resulting from the simulation of the second and the third CRN configurations matches the NO field monitoring measurements. Note that the NO concentration given by the first configuration underpredicts, in about 3.20 ppm, the NO measured data, representing a deviation of approximately 20%. Finally, it is assumed that the three configurations reproduce correctly the CO emissions; this is supported by the fact that there is not a measurement technique that could measure CO concentrations that are below of 1 ppm with sufficient accuracy.

Figures 7 and 8 display, respectively, the comparisons of the evolution of the temperature and CO and NO concentrations within the combustor. Note, from Fig. 7, that the evolution of the temperature at the intermediate and dilution zones estimated by the first and third configurations (or cases) are the same. However, there is a perceptible discrepancy in the prediction of the temperature in the primary zone given by the second configuration, when it is compared with the others arrangements.

An investigation on the primary zone shows a considerable increase of temperature computed with the second configuration [53], which has an impact over the combustion process along the intermediate and dilution zones, conducing to values of temperature that are approximately 20 K greater than the other configurations. This indicates that the normal distribution of the primary zone

Table 5 Global operational parameters at base load operation considered for the simulation of the combustor by the use of three CRN approaches

Entrance Parameters		Units	Value	Natural gas composition	
Air	Total mass flow	kg/s	22.9	Chemical species	% molar
	Pressure	MPa	1.6	Methane	96.100
	Temperature	°C	420	Ethane	1.600
Natural gas	Total mass flow	g/s	600	Propane	0.410
	Pressure	MPa	3.3	iso-Butane	0.077
	Temperature	°C	136	*n*-Butane	0.089
Feeding System [a]	Stage A	%	42.96	iso-Pentane	0.027
	Stage B	%	43.04	*n*-Pentane	0.019
	Stage C	%	7.48	*n*-Hexane	0.026
	Pilot stage	%	6.52	Nitrogen	1.057
				Carbon dioxide	0.595
				Total	100.000

[a]Natural gas feeding system distribution among the stages obtained from field data.

Table 6 Distribution for natural gas mass flow rate, PSR volume, and mass flow percentages rate applied to the third configuration by adjusting the CRN approach against the gas turbine data

Stages	NG mass flow rate, g/s	PSR volume, cm^3	Air mass flow percentage, %
Stage A	264.4	7162	47
Stage B	266.6	7162	47
Pilot Stage	44.5	4775	6
Stage C	45.5	-	-
Total	621	19099	100

Table 7 Comparisons of the thermochemical parameters at the exit of the transition piece in the simulation of the combustor at base load regime (169.17 MW) by the use of the three CRN approaches

Parameter	Chemical reactor network approaches			Gatecycle[a] or field data[b]
	First configuration	Second configuration	Third configuration	
Temperature, K	1626	1648	1626	1628[a]
CO (ppm at 15% O_2)	0.6	0.8	0.6	0.9[b]
NO (ppm at 15% O_2)	12.0	15.5	15.5	15.2[b]

[a]From GateCycle™ software.
[b]Field data.

equivalence ratio represented by 9 PSRs, calculated previously for this specific combustion chamber, leads to temperature values that are superior than those obtained with the first configuration, i.e., by the simulation of the primary zone as being modeled by a single PSR.

Figure 8 represents the evolution of the CO and NO concentrations along the combustor. Note in Fig. 8a that the CO concentrations predicted by the three configurations in the primary zone is higher than those found after the dilution with air that occurs in the subsequent zones. Furthermore, there is a substantial difference, that reaches 600 ppm of CO concentration, between the first and the second configurations, nevertheless, this strong discrepancy tends to decrease as the combustion products go through the intermediate and dilution zones, until the values at the end of the combustion chamber which its discrepancy does not reach 0.3 ppm.

Finally, Fig. 8b shows the NO evolution along the combustion chamber. In this figure, it is possible to verify that the NO formation is initiated in the primary zone of the combustor and its concentration decreases slightly as the burnt gases pass through the intermediate and dilution zones. So, it can be stated that NO formation is strongly influenced by the combustion process in the primary zone, which has a direct impact on the NO emissions at the exit of the combustion chamber.

The comparison between the temperature (Fig. 7) and the NO emissions (Fig. 8b) evolution in the primary zone reveals the inexistence of a correlation among these parameters. This analysis highlights the importance of the correct description of the mixing process within the primary zone combustion chamber to reach a good estimate of the NO emissions. Specifically, the CRN model that considers the primary zone as being represented by a single PSR (first configuration) is not suitable for the description of this process, whereas the second and third configurations adequately predicts the CO and NO emissions.

On the basis in the comparative results among the three configurations previously shown, the one that individualizes the several natural gas feeding systems (stages) demonstrated a higher competence in reproducing the temperature values as well as the NO and CO concentrations at the exit of the combustion chamber. Therefore, on the subsequent sections of this work, the third configuration will be used (as can be seen in Fig. 6) to study the influence of the natural gas composition as well as the stage fuel distribution on the thermochemical parameters at the end of the combustion process, i.e., at the exit of the combustor.

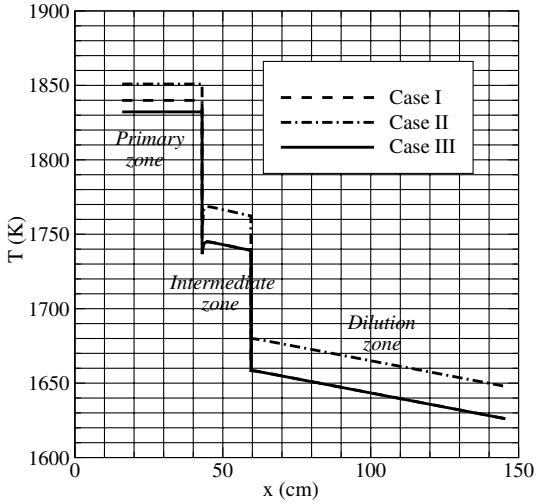

Fig. 7 Comparisons of the temperature's profile at the inner of the combustor as a result of the simulation considering the tree CNR's methodologies.

B. Influence of Natural Gas Composition on the Thermochemical Parameters

In this section, the influence on temperature and CO and NO emissions at the exit of the combustion process as a response of the

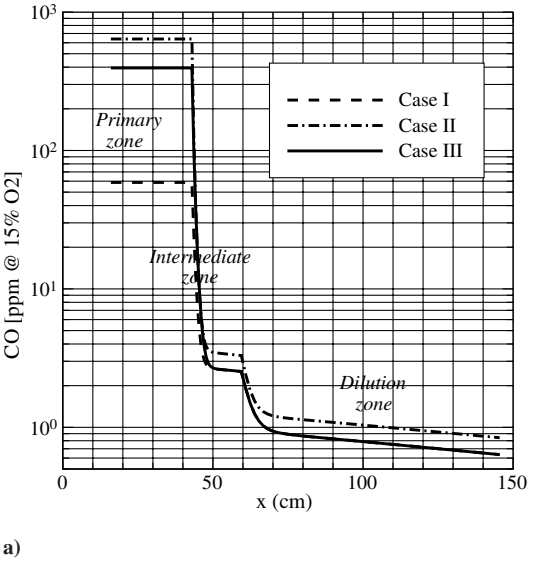

a)

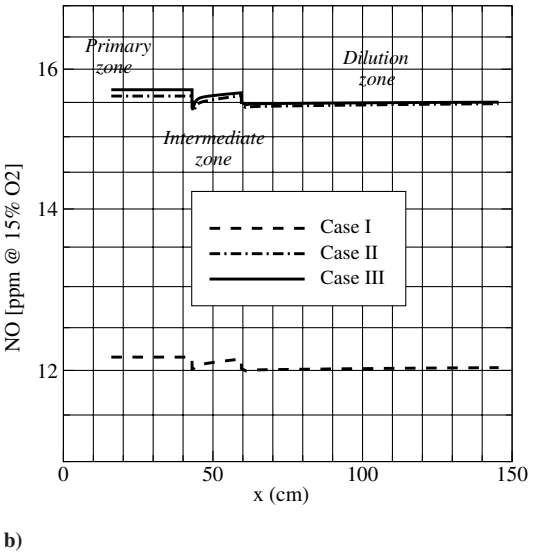

b)

Fig. 8 Comparisons of the a) carbon monoxide and b) nitrogen oxide profile at the inner of the combustor as a result of the simulation considering the three CNR's methodologies.

natural gas composition variation for the present combustor operating at three conditions will be shown and discussed. This was previously described in Table 4, i.e., one *base load* regime with evaporative-cooler off (169.17 MW), and two different *part load* regimes (144.01 and 149.15 MW). Note that these power levels correspond to the nominal natural gas composition. The present work examines the influence of natural gas composition for fixed compressor outlet conditions, therefore, it is expected that the actual power level varies with natural gas composition.

For this purpose, several natural gas compositions will be considered in this work, (see Table 1) for the subsequent simulations to represent the possible variations in the composition of the natural gas. It is important to recall that the obtained linear regression considers a set of 489 natural gas compositions, which represents the variation in the history of the measured concentrations along 489 days, in which a gas turbine installation was provided with this gaseous fuel.

The principal initial parameters for the simulation of the combustion process for each operating condition are those obtained by the thermodynamic simulation using the GateCycle™ software, referring to the global operation parameters like pressure, mass flow and temperature for air and natural gas. The measured mass flow distribution among the four stages in a DLN combustor was extracted from the gas turbine data.

Initially, the results obtained by the simulation with Chemkin™ are compared with those determined by the use of the GateCycle™ software as well as the emission data supplied by a gas turbine installation at the same three operation regimes. This allows to validate the selected CRN configuration for each operating condition. It is worth to emphasize that the last configuration is already validated in the previous section, base load regime (169.17 MW).

1. *Base Load Regime (169.17 MW)*

The first case to be studied corresponds to the combustion process at *base load* regime (169.17 MW). The inlet parameters needed for the simulation under this operation condition are shown in Table 7. Notice that those values correspond to a single gas turbine combustion chamber.

The results corresponding to the simulation of the third CRN configuration are depicted in Fig. 9, with the main purpose of assesing the agreement between the results of temperature and CO and NO concentrations calculated with those estimated by the use of the GateCycle™ software and obtained by the emissions data for the DLN gas turbine.

Figure 9 also shows the results of the systematic variation of the natural gas composition (expressed in terms of the methane percentage) over temperature (Fig. 9a) and CO and NO emissions (Fig. 9b) at the exit of the combustion chamber at base load regime (169.17 MW). It can be seen, from Fig. 9a, a linear increment of 30.8 K, which corresponds to 1.9% when the methane concentration in the natural gas is increased from 92 to 98%. This behavior was expected to occur owing to the increment of the methane

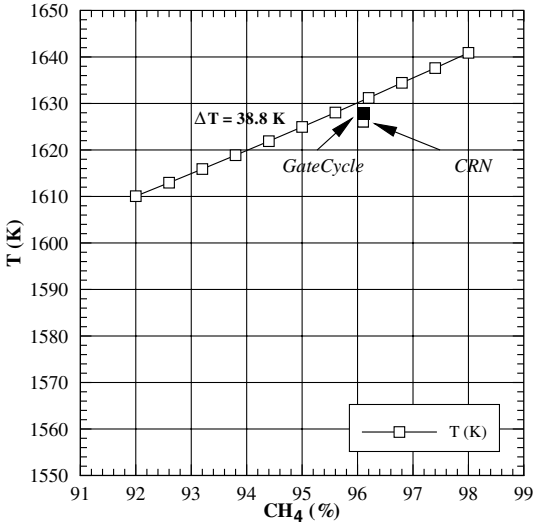

a)

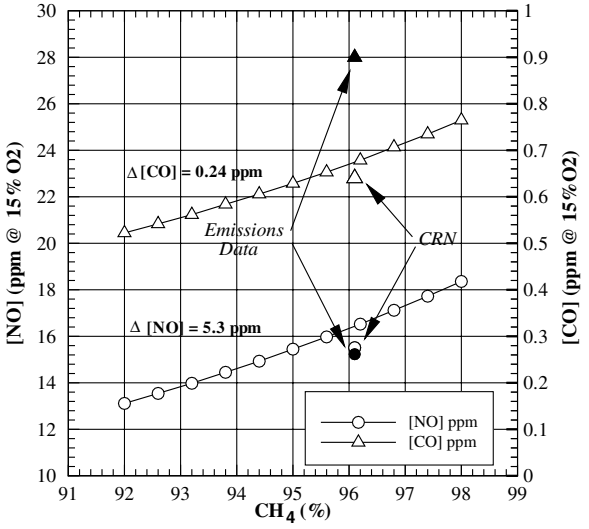

b)

Fig. 9 Influence of the methane composition on the a) temperature and b) CO and NO, at the exit of the combustion chamber in the GT operation. Nominal fuel composition corresponds to *Base Load* case (169.17 MW).

Table 8 Initial values used by the simulation of the combustion of a gas turbine combustion chamber at part load I regime (144.00 MW)

Entrance Parameters		Units	Value	Natural gas composition	
Air	Total mass flow	kg/s	21.1	Chemical species	% molar
	Pressure	MPa	1.46	Methane	96.100
	Temperature	°C	424	Ethane	1.660
Natural gas	Total mass flow	g/s	537	Propane	0.440
	Pressure	MPa	3.3	iso-Butane	0.080
	Temperature	°C	138	*n*-Butane	0.090
Feeding System[a]	Stage A	%	42.85	iso-Pentane	0.030
	Stage B	%	42.02	*n*-Pentane	0.020
	Stage C	%	7.91	*n*-Hexane	0.030
	Pilot stage	%	7.22	Nitrogen	1.010
				Carbon dioxide	0.610
				TOTAL	100.000

[a]Natural gas feeding system distribution among the stages obtained from field data.

Table 9 Results of temperature and emission obtained from the CRN simulation of a DLN gas turbine combustor operating at part load I regime (144.00 MW)

Exit parameters	Third CRN configuration	GateCycle™	GT emission data
Temperature, K	1603	1611	——
[NO] (ppm at 15% O_2)	25.4	--	20.5
[CO] (ppm at 15% O_2)	0.5	--	0.4

concentration that leads to the linear increase in its lower heating value. Note that, as the combustion temperature increases, the turbine output also increases.

The evolution of NO concentration (normalized in a dry basis of 15% of O2) with the natural gas composition (percentage of methane) is shown in Fig. 9b, which reveals an increment of 5.2 ppm that represents an increase of about 40% the NO concentration to be expected by the use of 92% of methane. The increment of NO observed with the increase of the methane composition in the natural gas suggests the predominance of the thermal NO mechanism over the others mechanisms in the description of the NO formation owing to the fact that an increment in the composition of methane in natural gas leads to an increase in temperature of the burnt gases that are present within the primary zone of the combustion chamber.

Also, Fig. 9b shows the evolution with the natural gas composition of the CO concentration at the exit of the combustor. It can be noted that the concentration of CO does not overcome the 1.0 ppm, and that the variation of CO with the concentration of methane is practically negligible, reaching only an increment of 0.19 ppm as the methane concentration in natural gas increases from 92 to 98%.

2. *Part Load I Regime (144.00 MW)*

Table 8 displays the values used in the CRN simulation relevant to the functioning of the combustor when operating in a *part load* condition (144.00 MW), herein called as *part load I* regime. It is worth to stress out that the global operational parameters of the combustion chamber (i.e., pressure, temperature, mass flow of reactants) were estimated using the model of the gas turbine developed in the GateCycle™. The natural gas distribution over the four fuel injection stages was taken from the data given by the gas turbine installation.

The burnt gas temperature, CO and NO emission at the end of the combustion process in the operation of the gas turbine at *part load I* regime (144.00 MW) were obtained by the use of the third CRN configuration, and compared with those yielded by the GateCycle™ model and the emission data from the gas turbine installation, as can be seen in Table 9 and depicted in Fig. 10. Notice, from Table 9 and Fig. 10, that a small of difference of 7 K was found in the temperature of burnt gases at the end of the combustion chamber, that represents a 0.5% variation of the temperature when both approaches are considered.

Concerning to the pollutant emissions, it can be observed that the CO concentration estimated by the CRN simulation exhibits a value that is in a perfect agreement with the one obtained by the gas turbine emission data. However, the NO concentration calculated in this work reveals a value that is 5 ppm higher than that one reported by the monitoring of the GT installation, representing a discrepancy that reaches 25% in the prediction of the NO emissions.

Figure 10 also depicts the influence in the variation of composition of natural gas, (expressed by the volumetric percentage of methane contained in the NG) on the thermochemical parameters at the end of the combustion process at part load I regime (144.00 MW). The results obtained from the CRN simulation show a linear increase of the temperature of burnt gases at the exit of the transition piece equivalent to 30 K (1.89%) when the natural gas composition is altered according the sequence shown in Table 1. Note that this increment of 30 K is practically similar to that estimated for the *base load* case.

As can be seen in Fig. 10b, the NO concentration increases 8 ppm (38%) when natural gas concentration changes from 92 to 98% in methane composition. This increment of 8 ppm is greater than that obtained in *base* load condition (Fig. 9b), even though the burnt gases temperatures at the end of the combustor chamber operating at *part load I* regime is lower than that encountered at *base load* operation condition. Note that this last statement seems to be contradictory to a previous one where the total NO formation was deemed strongly influenced by the thermal mechanism and, therefore, by the primary zone temperature. Nevertheless, a reduction of gas turbine load corresponds to an increase in the percentage of natural gas that flows through the pilot stage which operates at higher temperatures.

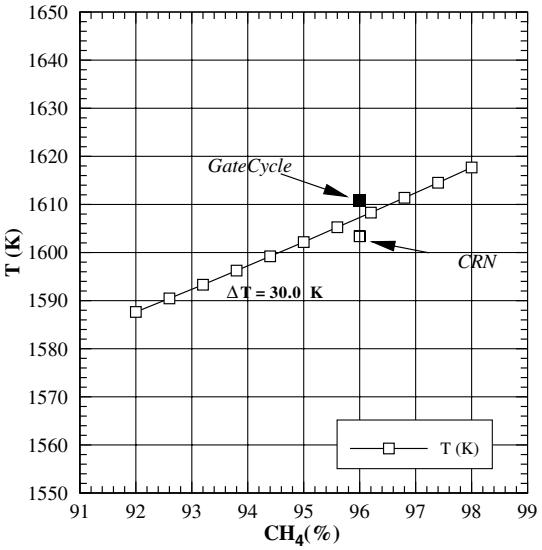

a)

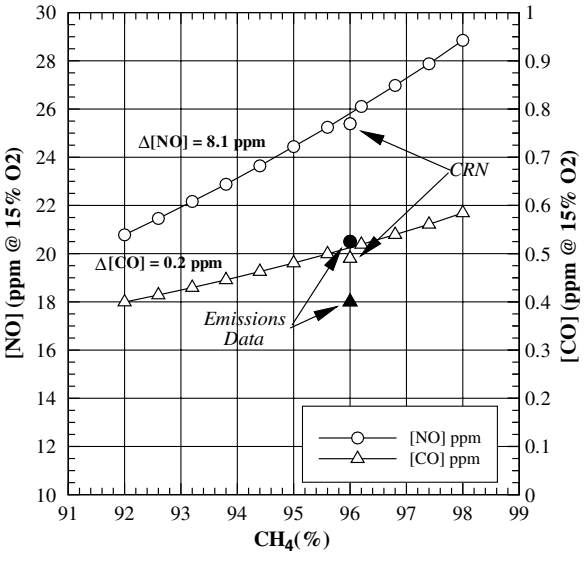

b)

Fig. 10 Influence of the methane composition on the a) temperature and b) CO and NO, at the exit of the combustion chamber in the GT operation. Nominal fuel composition corresponds to *Part Load I* case (144.00 MW).

Table 10 Initial values used by the simulation of the combustion chamber at part load II regime (149.00 MW)

Entrance Parameters		Units	Value	Natural gas composition	
Air	Total mass flow	kg/s	21.8	Chemical species	% molar
	Pressure	MPa	1.39	Methane	97.200
	Temperature	°C	409	Ethane	1.380
Natural gas	Total mass flow	g/s	542	Propane	0.240
	Pressure	MPa	3.3	iso-Butane	0.025
	Temperature	°C	138	*n*-Butane	0.035
Feeding System[a]	Stage A	%	42.85	iso-Pentane	0.005
	Stage B	%	43.18	*n*-Pentane	0.005
	Stage C	%	7.52	*n*-Hexane	0.005
	Pilot stage	%	6.45	Nitrogen	0.765
				Carbon Dioxide	0.405
				Total	100.000

[a]Natural gas feeding system distribution among the stages obtained from field data.

Table 11 Results of temperature and emission obtained from the CRN simulation of a DLN gas turbine combustor operating at part load II regime (149.00 MW)

Exit parameters	Third CRN configuration	GateCycle™	GT emission data
Temperature, K	1591	1592	——
[NO] (ppm at 15% O_2)	22.1	--	20.5
[CO] (ppm at 15% O_2)	0.4	--	0.4

Figure 10b also shows a small increment in the CO concentration equivalent to 0.19 ppm as the methane composition in the natural gas is changed from 92 to 98%.

3. *Part Load II Regime (149.00 MW)*

The third case to be addressed corresponds to the determination of the thermochemical parameters of the gas turbine combustor operating at part load regime equivalent to 149.00 MW, which will be dubbed here as *part load II* regime. As can be seen in Table 10, the global parameters for this regime are similar to those considered for the *part load I* regime, reason for that, this section will be limited to providing a brief description of the results obtained by the CRN simulation of the combustor at this specific operational condition.

Table 11 shows the results of the simulation of the combustion process of the combustor for the case of part load II (149 MW), in comparison to the temperature at the end of the combustion process calculated by GateCycle™ and the emission data provided by the gas turbine installation.

Note, from Table 11, that an excellent agreement is observed referring to the burnt gases temperature and CO concentration obtained by the application of the third CRN configuration, when compared with the results obtained by the use of GateCycle™, and the CO concentration measured in the gas turbine installation. A small disagreement is observed on the NO concentration provided by both approaches, where the simulated value of NO concentration is 1.6 ppm superior to the measured value, which represents a discrepancy that does not overcome 8%.

Figure 11 depicts the burnt gases temperature and emission evolution at the end of the DLN combustor with the variation of the natural gas that is feeding to the combustion primary zone, when the gas turbine is operating at part load II regime (149 MW). Figure 11a shows an increment of 29 K (1.9%) for the burnt gases temperature at the exit of the transition piece, when the methane concentration in the natural gas is increased from 92 to 98%. Note that this rise for the burnt gases temperature at the end of the combustion process is found to be similar to that obtained for the case of part load I regime.

Moreover, Fig. 11b shows the existence of a 6.7 ppm (41%) increase in the NO concentration when the methane composition in the natural gas is varied from 92 to 98%. A comparison of Fig. 10b with Fig. 11b evidences a similarity in the NO concentration variations when the gas turbine is operated under part load regime within the range of 144–149 MW.

Finally, a small increment of the CO concentration, equal to 0.14 ppm, can be also observed in Fig. 11b when the composition of methane in the gas natural is modified from the minimum to the maximum value. It is believed that from the practical and regulatory perspective, the absolute values of CO concentration and the relative variation are not of great significance.

4. *Parametric Study*

This section summarizes the results obtained for the three different load conditions, ranging from base load (169.17 MW) to minimum load (144.00 MW). The comparison of Figs. 9–11, that the burnt gases temperature at the combustion chamber exit is an increasing function of the methane concentration of the natural gas. These figures also permit to verify the direct proportionality between the power of the gas turbine and the increment of the burnt gases temperature at the combustion chamber exit. In other words, as the power of the gas turbine decreases, also diminishes the temperature variation when the methane composition in the natural gas increases.

Similarly, these figures also display the CO and NO concentrations at the end of the combustion process for the three previously analyzed gas turbine operation regimes. Notice the similar behavior for the CO evolution and for the temperature, i.e., high values in the CO emissions as a consequence of the variation of the composition of the natural gas are obtained in situations where burnt gases temperature at the exit of the combustor chamber are higher.

An analysis of the individual behavior of each reactor stage shows that, when methane content increases, the stage combustion temperature always increases. The combustion temperature is close to 2100 K for the pilot stage (because the mixture composition is far away from the lean extinction limit), and close to 1800 K for A and B stages (which composition lies close to the lean extinction limit of the PSR). As a consequence, CO concentration decreases with temperature in stages A and B and increases in the pilot stages. The combined result in the primary combustion zone, is a slight increase of CO at the combustor exit as the methane volumetric percentage in the natural gas increases. Note that the ascending behavior of CO at the pilot stage is related to the high-temperature combustion, which leads to the formation of CO via CO_2 dissociation caused by the backward reaction $CO + OH \Leftrightarrow CO_2 + H$.

It is also worthwhile to emphasize that the absolute values in the CO concentrations encountered are smaller than 1 ppm. Therefore, even if the percentage variations with the natural gas composition

could be important, their range does not attract the attention from the point of view of the environmental regulations.

Furthermore, NO concentration at the exit of the combustor is strongly increased when the natural gas methane concentration increases from 92 to 98%, which is mainly due to the corresponding augment of combustion temperature.

C. Analysis of the Stage Fuel Distribution

Because the gas turbine combustion chamber analyzed in this work operates with four feeding systems, also called stages (A, B, C and Pilot), in this section, will be analyzed the influence that produces the change in the natural gas flow that enters each stage, on the burnt gases temperature and emissions at the exit of the combustor.

To carry out this analysis, it was considered the operation of the gas turbine at base load regime (as shown in Table 6). The natural gas distribution was altered following 11 possible paths, also called cases in the supply of natural gas to the primary zone of the combustor, as can be seen in Fig. 12, which corresponds to the realistic natural gas distribution reported by the gas turbine installation for three different operational regimes:

1) *Base load*: (169.17 MW) designated as case 1.
2) *Part load I*: (149.00 MW) designated as case 6.
3 *Part load III*: (109.70 MW) designated as case 11.

The remaining eight cases were obtained by linear interpolation of these three cases and are considered as the building blocks in the subsequent simulation, because they represent, approximately, the possible range of operation of the GT (109.17–169.70 MW) in study. The natural gas mass flow rate is 600 g/s. It is important to emphasize that the air mass flow of the remaining eight cases is the same as the three baseline cases to maintain the same equivalence ratio.

Figure 13 shows the results of the burnt gases temperature and the CO and NO emissions at the end of the combustor as a function the variation in the gas natural supply (designated by cases) in the four stages (as show in Fig. 12).

On the basis of the results shown in Fig. 13, it was found an absence of variation in the results related to the temperature and CO concentrations in all the 11 cases considered in this simulation. Nonetheless, the NO concentration is notably increased in the cases where there is an increment in the mass flow in the Pilot stage and stage C. Such increases lead to high levels of NO (36.6 ppm at

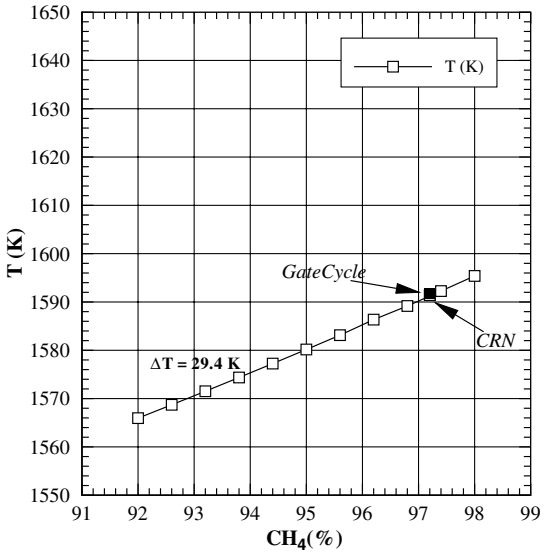

a)

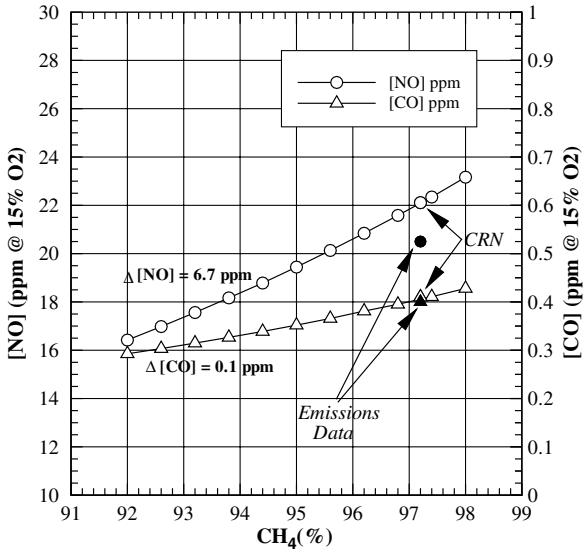

b)

Fig. 11 Influence of the methane composition on the a) temperature and b) CO and NO, at the exit of the combustion chamber in the GT operation. Nominal fuel composition corresponds to *Part Load II* case (149.00 MW).

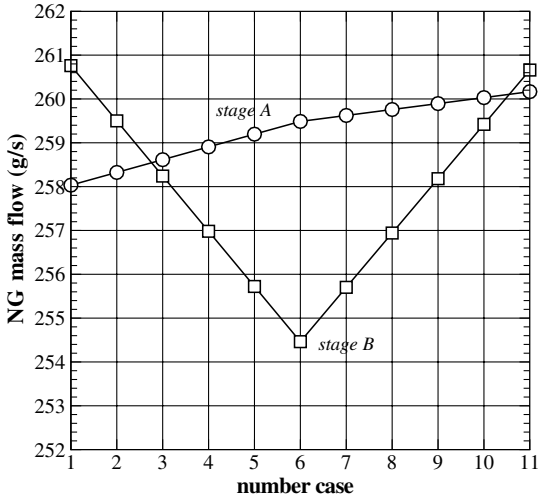

a)

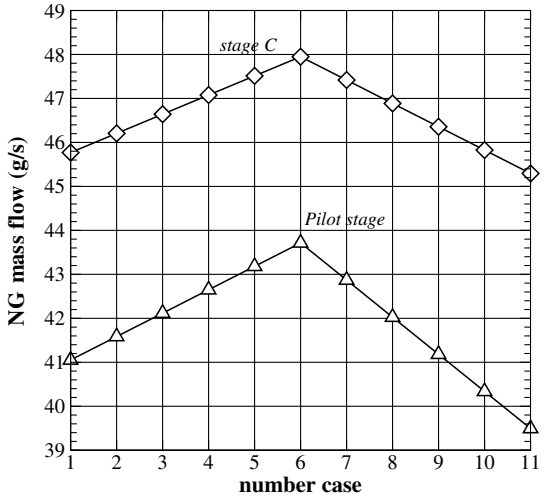

b)

Fig. 12 Natural gas mass flow variations distributed to the 4 feeding systems (stages) of the gas turbine combustor considering 11 possible situations.

15% O_2) when the mass flown in stage C and Pilot stage reach 47.95 g/s (7.92%) and 43.72 g/s (7.22%), respectively. It is believed that the mass flow in Pilot stage is primarily responsible for the great sensitivity encountered in the NO formation, because an increase of 10.69% of natural gas that is injected in the pilot stage leads to an increment of 130% in the NO concentration at the exit of the combustor chamber. Note that the increase of natural gas concentration in the stage C affects simultaneously stages A, B, and Pilot.

The strong sensitivity exhibited by the NO concentration as a function of the mass flow in the four stages can be verified further in Fig. 13, which shows the variation with the temperature of the NO concentration formed in the primary zone, by the stages A, B and Pilot. The temperatures calculated for the stages A and B in the primary zone combustion are approximately 200 K smaller than the estimated temperature corresponding to the combustion downstream the Pilot stage. These differences in the temperature are propagated in the NO prediction in the primary combustion zone, where it can be perceived that NO concentration computed in the primary zone by the Pilot stage is more than two orders larger than the NO concentration that forms the combustion process in the stages A and B.

Thus, an increment of 4.22 g/s (10.69%) of natural gas that is provided to the pilot stage leads to and increment of 108.6 K in the burning temperature, resulting in an increase of 711 ppm of NO (185%). In the case of the combustion in the stages A and B, and increment of 6.88 g/s of natural gas drives to an increase of 16.7 K the combustion temperature, and consequently, an augment of 1.12 ppm of NO (18%).

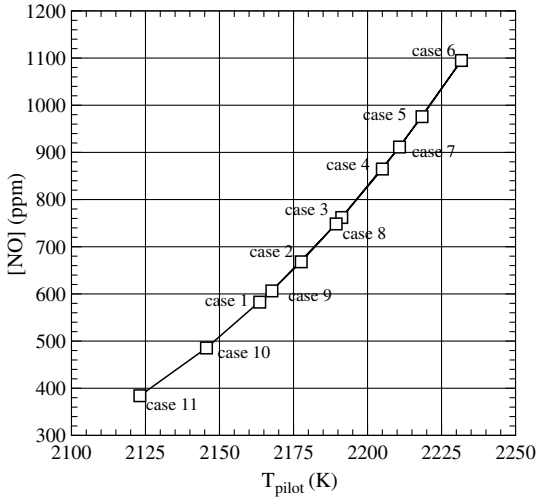

a)

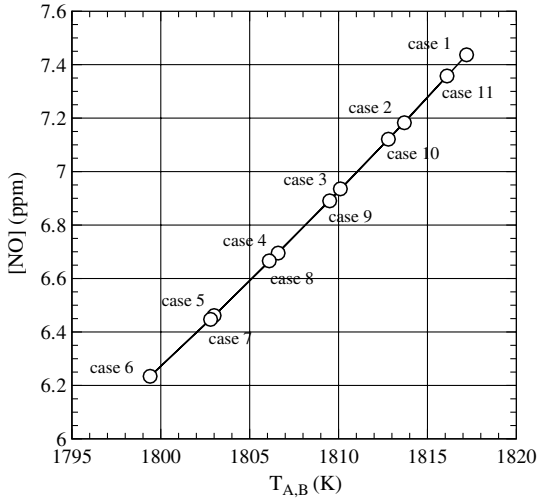

b)

Fig. 13 NO evolution provided by (top) the combustion in the pilot stage and (bottom) the combustion A and B, when considering a variation in the natural gas system in accord to the 11 presented situations.

VII. Conclusions

This work described the combustion modeling of a gas turbine to predict the temperature and concentrations of CO and NO at the end of the combustion process for different gas turbine loads. For this purpose, one of the 16 gas turbine combustors was considered as representative for the purposes of this modeling using several methodologies of solution under the context of the CRN approach. This approach allows reducing the level of complexity of the governing fluid mechanics equations, whereas retaining a detailed description of the reactions of combustion. It is worth emphasizing that, among several mechanisms investigated, the L&D mechanism was found to be the most suitable to describe combustion within PSRs, which justifies its use in this work.

Thus, for the modeling of the combustion chamber of a typical industrial gas turbine, the geometrical configuration was approximated to investigate three configurations, typical of the CRN approach. Moreover, it was chosen the one that considers the details of the operation of the combustor, which permits to give a good estimate on the evolution of the thermochemical parameters of the combustion process in *base load* condition. In this case, the composition of the gas considered in the simulation was that measured under actual operational conditions

After that, the most suitable CRN configuration in *base load* regime was chosen and other gas turbine operational regimes were considered (144.00 and 149.00 MW) to determine the impact of fuel composition on the concentration of pollutants. By comparing the calculated results with the measured values of concentration of NO and CO, It can be concluded that the third CRN configuration is able to predict properly the thermochemical parameters of interest in these operation conditions.

Thus, under these operation conditions of the turbine, it was determined that an increase in the concentration of methane in natural gas within the range of 92–98% involves an increase in temperature within the range of 1.88–1.91% whereas the CO at the exit of the combustion chamber increased from 0.14–0.19 ppm. The increased emissions of NO as a result of increased concentration of methane in natural gas are influenced by temperature in the primary zone of combustion and by the distribution of natural gas in the several feeding stages. In particular, high NO concentrations were found as the mass flow rate of natural gas is increased in the pilot stage. Moreover, it was demonstrated the increment in NO concentration between 39.21 and 41.06% as the concentration of methane in natural gas is increased from 92 to 98%.

Finally, it is important to emphasize the inherent limitation in the use of the CRN approach in the simulation of combustion as the result of the simplification on the fluid mechanics equations, in contrast to the more elaborate description of the kinetic of combustion and the lower computational burden. A good alternative in the modeling and simulation of practical combustion systems as DLN gas turbine combustors could be the adoption of sophisticated approaches, complementary to the CRN approach, such as the CFD, to get a better prediction of the thermochemical process in such combustion devices.

Acknowledgments

This work was supported by a discretionary grant of Usina Termelétrica Norte Fluminense, Brazil, under the auspicious of Agência Nacional de Energia Elétrica, Research and Development Program, and performed while Luís Fernando Figueira da Silva was a Visiting Professor, funded by the National Petroleum Agency (Brazil), on leave from Centre National de la Reserche Scientifique, France.

References

[1] Lee, J. C. Y., Malte, P., and Nicol, D. G., "NOx as a Function Type: C1-to-C16 Hydrocarbons and Ethanol," *44th International Gas Turbine and Aeroengine Congress*, American Society of Mechanical Engineers Paper No 99-GT-270, 1999, pp. 272–280.

[2] Malte, P., Edmonds, R., Lee, A. C., Novosselov, I., Polagye, B., and Fackler, K. B., "NOx from Gaseous and Prevaporized Fuel Burned Lean-Premixed at Atmospheric Pressure in Single-Jet Stirred Reactor," *5th US Combustion Meeting, Western States Sections of the Combustion Institute*, The Combustion Inst., Paper No. E38, 2007, pp. 1–22.

[3] Hack, L. R., and McDonnel, V. G., "Impact of Ethane, Propane and Diluent Content in Natural Gas on the Performance of a Commercial Microturbine Generator," *Journal of Engineering for Gas Turbine and Power*, Vol. 130, No. 1, 2008, pp. 011509:1–7.

[4] Erbes, M. R., Gay, R. R., and Cohn, A., "GATE: A Simulation Code for Analysis of Gas-Turbine Power Plants," *ITGI/ASME Gas Turbine Congress*, American Society of Mechanical Engineers, Fairfield, NJ, 1989, pp. 1–19.

[5] Law, C. K., Sung, C. J., Wang, H., and Lu, T. F., "Development of Comprehensive Detailed and Reduced Mechanism for Combustion Modeling," *AIAA Journal*, Vol. 41, No. 9, 2003, pp. 1629–1646. doi:10.2514/2.7289

[6] Bowman, C. T., "An Experimental and Analytical Investigation of the High Temperature Oxidation Mechanisms of Hydrocarbon Fuels," *Combustion Science and Technology*, Vol. 2, Nos. 2–3, 1970, pp. 161–172. doi:10.1080/00102207008952244

[7] Cooke, D. F., and Williams, A., "Shock-Tube Studies of the Ignition and Combustion of Ethane and Slightly Rich Methane Mixtures with Oxygen," *13th Symposium International on Combustion*, Vol. 13, No. 1, Combustion Inst., Pittsburgh, PA, 1971, pp. 757–766. 10.1016/S0082-0784(71)80078-4

[8] Westbrook, C. K., Dryer, F. L., and Schug, K. P., "A Comprehensive Mechanism for the Pyrolisis and Oxidation of Ethylene," *19th Symposium International on Combustion*, Vol. 19, No. 1, Combustion Inst., Pittsburgh, PA, 1982, pp. 153–166. 10.1016/S0082-0784(82)80187-2

[9] Westbrook, C. K., and Dryer, F. L., "Chemical Kinetics Modeling of Hydrocarbon Combustion," *Progress in Energy and Combustion Science*, Vol. 10, No. 1, 1984, pp. 1–57. doi:10.1016/0360-1285(84)90118-7

[10] Dagaut, P., Lecomte, F., Chevailler, S., and Cathonnet, M., "Experimental and Detailed Kinetic Modeling of Nitric Oxide Reduction by a Natural Gas Blend in Simulated Reburnig Conditions," *Combustion Science and Technology*, Vol. 139, No. 1, 1998, p. 329. doi:10.1080/00102209808952093

[11] Glarborg, P., Miller, J. A., and Kee, R. J., "Kinetic Modeling and Sensitivity Analysis on Nitrogen Oxide Formation in Well Stirred Reactors," *Combustion and Flame*, Vol. 65, No. 2, 1986, pp. 177–202. doi:10.1016/0010-2180(86)90018-0

[12] Miller, J. A., and Bowman, C. T., "Mechanism and Modeling of Nitrogen Chemistry in Combustion," *Progress in Energy and Combustion Science*, Vol. 15, No. 4, 1989, pp. 287–338. doi:10.1016/0360-1285(89)90017-8

[13] Baulch, D. L., Cobos, C. J., Cox, R. A., Esser, C., Frank, P., Just, T., Kerr, J. A., Murrels, T., Pilling, M. J., Troe, J., Walker, R. W., and Warnatz, J., "Evaluated Kinetic Data for Combustion Modeling. Supplement I," *Journal of Physical and Chemical Reference Data*, Vol. 21, No. 3, 1992, pp. 411–734. doi:10.1063/1.555908

[14] Baulch, D. L., Cobos, C. J., Cox, R. A., Frank, P., Hayman, G., Just, Th., Kerr, J. A., Murrels, T., Pilling, M. J., Troe, J., Walker, R. W., and Warnatz, J., "Sumary Table of Evaluated Kinetic Data for Combustion Modeling: Supplement I," *Journal of Physical and Chemical Reference Data*, Vol. 23, No. 6, 1994, pp. 847–848. doi:10.1063/1.555953

[15] Baulch, D. L., Cobos, C. J., Cox, R. A., Just, Th., Kerr, J. A., Murrels, T., Pilling, M. J., Stocker, D., Troe, J., Tsang, W., Walker, R. W., and Warnatz, J., "Evaluated Kinetic Data for Combustion Modeling: Supplement II," *Journal of Physical and Chemical Reference Data*, Vol. 34, No. 3, 2005, pp. 757–1397.

[16] Frenklach, M., Wang, H., and Rabinowitz, M., "Optimization and Analysis of Large Kinetic Mechanism Using the Solution Mapping Method: Combustion of Methane," *Progress in Energy and Combustion Science*, Vol. 18, No. 1, 1992, pp. 47–73. doi:10.1016/0360-1285(92)90032-V

[17] Hughes, K. J., Tomlin, A. S., Dupont, V. A., and Pourkashanian, M., "Experimental and Modelling Study of Sulfur and Nitrogen Doped Premixed Methane Flames at Low Pressure," *Faraday Discussions*, Vol. 119, No. 1, pp. 337–352. doi:10.1039/b102061g

[18] Frenklach, M., Wang, H., Goldenberg, M., Smith, G. P., Golden, D. M., Bowman, C. T., Hanson, R. K., Gardiner, W. C., and Lissianski, V., "GRI-Mech -An Optimized Detailed Chemical Reaction Mechanism for Methane Combustion," GRI-Mech, GRI-95/0058, 1995.

[19] Hughes, K. J., Turányi, T., Clague, A. R., and Pilling, M. J., "Development and Testing of a Comprehensive Chemical Mechanism for the Oxidation of Methane," *International Journal of Chemical Kinetics*, Vol. 33, No. 9, 2001, pp. 513–538. doi:10.1002/kin.1048

[20] Simmie, J. M., "Detailed Chemical Kinetics Models for the Combustion of Hydrocarbon Fuels," *Progress in Energy and Combustion Science*, Vol. 29, No. 6, 2003, pp. 513–538.

[21] Borisov, A. A., Dragalova, E. M., Zamanskii, V., Lisyankii, V., and Skachkov, G. I., "Kinetics and Mechanism of Methane Self Ignition," *Khimicheskaia Fizika*, Vol. M4, 1982, pp. 536–543.

[22] Borisov, A. A., Zamanskii, V., Lisyanskii, V., and Rusakov, S. A., "High-Temperature Methanol Oxidation," *Soviet Journal of Chemical Physics*, Vol. 9, No. 8, 1992, pp. 1836–1849.

[23] Borisov, A. A., Zamanskii, V., Konnov, V. M., Lisyanskii, V., Rusakov, S. A., and Skachkov, G. I., "High-Temperature Ethanol Ignition," *Soviet Journal of Chemical Physics*, Vol. 9, No. 8, 1992, pp. 2527–2537.

[24] Konnov, A. A., "Detailed Reaction Mechanism for Small Hydrocarbon Combustion," Release 0.5, 2000, http://homepages.vub.ac.be/-akonnov/,

[25] Davidenko, D., "Contribution au Développement des Outils de simulation Numérique de la Combustion Supersonique," Thèse de Doctorat, Université d Órleans, Orleans, France, 2005.

[26] Petrova, M. V., and Williams, F. A., "A Small Detailed Chemical-Kinetic Mechanism for Hydrocarbon Combustion," *Combustion and Flame*, Vol. 144, No. 3, 2006, pp. 526–544. doi:10.1016/j.combustflame.2005.07.016

[27] Balakrishnan, G., and Williams, F. A., "Turbulent Combustion Regimes for Hypersonic Propulsion Employing Hydrogen-Air Diffusion Flames," *Journal of Propulsion and Power*, Vol. 10, No. 3, 1994, pp. 434–436. doi:10.2514/3.23754

[28] Rightley, M. L., and Williams, F. A., "Burning Velocities of CO Flames," *Combustion and Flame*,Vol. 110, No. 3, 1998, pp. 285–297.

[29] Rightley, M. L., and Williams, F. A., "Structures of CO Diffusion Flames near Extinction," *Combustion Science and Technology*, Vol. 125, Nos. 1–6, 1997, pp. 181–200. doi:10.1080/00102209708935659

[30] Tan, Y., Dagaut, P., Cathonnet, M., Boettner, J. C., Bachman, J. S., and Carlier, P., "Natural Gas Blend Oxidation and Ignition: Experiments and Modeling," *Proceedings of the Combustion Institute*, Vol. 25, No. 1, 1994, pp. 1563–1569.

[31] Turbiez, A., Desgroux, P., Pauwles, J. F., Sochet, L. R., Poitou, S., and Perrin, M., "GDF-Kin: A New Step towards a Detailed Kinetic Mechanism for Natural Gas Combustion Modeling," *Proceedings of the 1998 International Gas Research Conference*, Gas Research Inst., San Diego, CA, Vol. 4, 1998, pp. 371–382.

[32] Tan, Y., Dagaut, P., Cathonnet, M., and Boettner, J. C., "Pyrolysis, Oxidation and Ignition of C1 and C2 Hydrocarbons: Experiments and Modeling," *Journal de Chimie Physique et de Physico-Chimie Biologique*, Vol. 92, Nos. 1–6, 1995, pp. 726–746.

[33] Voisin, D., "Cinétique Chimique d'Oxidation d´Hydrocarbures et Obtention dun Modèle pour la Combustion du Kérosene," Thèse, Université d Órleans, 1997.

[34] El Bakali, A., Dagaut, P., Pillier, L., Desgroux, P., Pauwles, J. F., Rida, A., and Meunier, P., "Experimental and Modeling Study of the Oxidation of Gas Natural in a Premixed Flame, Shock Tube and Jet Stirred Reactor," *Combustion and Flame*, Vol. 137, Nos. 1–2, 2004, pp. 109–128. doi:10.1016/j.combustflame.2004.01.004

[35] El Bakali, A., Desgroux, L. P., Lefort, B., Gasnot, L., Pauwles, J. F., and Costa, I. A., "NO Prediction in Natural Gas Flames Using GDF-Kin 3.0 Mechanism NCN and HCN Contribution to Prompt-NO formation," *Fuel*, Vol. 85, Nos. 7–8, 2006, pp. 896–909. doi:10.1016/j.fuel.2005.10.012

[36] Le Cong, T., and Dagaut, P., "Experimental and Detailed Kinetic Modeling of the Oxidation of Natural Gas, Natural Gas/Syngas, and Effect of Burnt Gas," *Energy Fuels*, Vol. 23, No. 2, 2009, pp. 725–734. doi:10.1021/ef800832q

[37] Dagaut, P., "On the Kinetics of Hydrocarbons Oxidation from Natural Gas to Kerosene and Diesel Fuels," *Physical Chemistry Chemical Physics*, Vol. 4, 2002, pp. 2079–2094. doi:10.1039/b110787a

[38] Le Cong, T., and Dagaut, P., "The Effect of Water Vapor on the Kinetics of Combustion of Hydrogen and Natural Gas: Experimental and Detailed Modeling Study," *Proceedings of GT2008*, American Society of Mechanical Engineers, Fairfield, NJ, 2008.

[39] Le Cong, T., "Etude Expérimentale et Modélisation de la Cinétique de Combustion de Combustibles Gaseux: Méthane, Gaz Naturel et Mélanges Contenant de l'Hydrogène, du Monoxyde de Carbone, du Dioxyde de Carbone et de l'Eau," Thèse de Doctorat, Université d'Orleans, 2007.

[40] Petersen, E. L., Kalitan, D. M., Simmons, S., Bourque, G., Curran, H. J., and Simmie, J. M., "Methane/Propane Oxidation at High Pressures and Detailed Chemical Kinetic Modelling," *Proceedings of the Combustion Institute*, Vol. 31, No. 1, 2007, pp. 447–454. doi:10.1016/j.proci.2006.08.034

[41] Healy, D., Kopp, M. M., Polley, N. L., Petersen, E. L., Bourque, G., and Curran, H. J., "Methane/Butane Ignition Delay Measurements at High Pressure and Detailed Chemical Kinetic Simulations," *Energy and Fuels*, Vol. 24, No. 3, 2010, pp. 1617–1627.

[42] Healy, D., Curran, H. J., Dooley, S., Simmie, J. M., Kalitan, D. M., Petersen, E. L., and Bourque, G., "Methane/Propane Mixture Oxidation at High Pressures and at High, Intermediate and Low Temperatures," *Combustion and Flame*, Vol. 155, No. 3, 2008, pp. 451–461. doi:10.1016/j.combustflame.2008.06.008

[43] Healy, D., Curran, H. J., Simmie, J. M., Kalitan, D. M., Zinner, C. M., Barrett, A. B., Petersen, E. L., and Bourque, G., "Methane/Ethane/Propane Mixture Oxidation at High Pressures and at High, Intermediate and Low Temperatures," *Combustion and Flame*, Vol. 155, No. 3, 2008, pp. 441–448. doi:10.1016/j.combustflame.2008.07.003

[44] Healy, D., Kalitan, D. M., Aul, C. J., Petersen, E. L., Bourque, G., and Curran, H. J., "Oxidation of C1–C5 Alkane Quinternary Natural Gas Mixtures at High Pressures," *Energy and Fuels*, Vol. 24, No. 3, 2010, pp. 1521–1528.

[45] Orbegoso, E. M., and Figueira da Silva, L. F., "On the Predictability of Chemical Kinetic Mechanisms for the Description Combustion of Gaseous Fuels," *20th International Congress on Mechanical Engineering*, Brazilian Society of Mechanical Sciences and Engineering, Rio de Janeiro, Brazil, 2009, pp. 1–11.

[46] Ruscic, B., Wagner, A. F., Harding., L. B., Asher, R. L., Feller, D., Dixon, D. A., Peterson, K. A., Song, Y., Quian, X., and Ng, C., "On the Enthalpy of Formation of Hydroxyl Radical Gas-Phase Bond Dissociation Energies of Water and Hydroxyl," *The Journal of Physical Chemistry A*, Vol. 106, No. 11, 2002, pp. 2727–2747. doi:10.1021/jp013909s

[47] Falcitelli, M., Pasini, S., and Tognotti, L., "Modelling Practical Combustion Systems and Predicting NOx Emissions with an Integrated CFD Based Approach," *Computers and Chemical Engineering*, Vol. 26, No. 9, 2002, pp. 1171–1183. doi:10.1016/S0098-1354(01)00771-2

[48] Nicol, D. G., Steele, R. C., Marinov, N. M., and Malte, P. C., "The Importance of the Nitrous Oxide Pathway to NOx in Lean-Premixed Combustion," *Transactions of the ASME*, Vol. 117, No. , 1995, pp. 100–111.

[49] Steele, R. C., Malte, P. C., Nicol, D. G., and Kramlich, J. C., "NOx and N2O in Lean Premixed Jet-Stirred Flames," *Combustion and Flame*, Vol. 100, No. 3, 1995, pp. 440–449.

[50] Steele, R. C., Jarrett, A. C., Malte, P. C., Tonouchi, J. H., and Nicol, D. G., "Variables Affecting NOx Formation in Lean-Premixed Combustion," *Transactions of the ASME*, Vol. 119, No. 1, 1997, pp. 102–107. doi:10.1115/1.2824074

[51] Rutar, T., Horning, D. C., Lee, J. C., and Malte, P. C., "NOx Dependency on Residence Time and Inlet Temperatures for Lean-Premixed Combustion in Jet-Stirred Reactors," *43th International Gas Turbine and Aeroengine Congress*, American Society of Mechanical Engineers, Fairfield, NJ, 1998.

[52] Adouane, B., "Low NOx Emissions from Fuel-Bound Nitrogen in Gas Turbine Combustors," Ph.D. Thesis, Technische Universiteit Delft, The Netherlands, 2006.

[53] Allaire, D. L., Waitz, I. A., and Wilcox, K. E., "A Comparison of Two Methods for Predicting Emissions from Aircraft Gas Turbine Combustors," *Proceedings of the ASME Turbo Expo 2007*, American Society of Mechanical Engineers, Fairfield, NJ, 2007.

[54] Risk, N. K., Chin, J. S., Marshall, A. W., and Razdan, M. K., "Predictions of NOx Formation Under Combined Droplet and Partially Premixed Reaction of Difusion Flame Combustors," *Journal of Engineering for Gas Turbines and Power*, Vol. 122, No. 1, 2002, pp. 31–38.

[55] Sturgess, G. J., Zelina, J., Shouse, D. T., and Roquemore, W. M., "Emissions Reduction Technologies for Military Gas Turbine Engines," *Journal of Propulsion and Power*, Vol. 21, No. 2, 2005, pp. 193–216. doi:10.2514/1.6528

T. Lieuwen
Associate Editor